IUST
Iran University of Science and Technology

Iranian Journal of Electrical and Electronic Engineering

Journal Homepage: ijeee.iust.ac.ir

Facilitating Winding Design and Performance Evaluation of WR Synchro

Mohamad Reza Eesazadeh*, Zahra Nasiri-Gheidari(C.A.)*

Abstract: This research focuses on electromagnetic position sensors, particularly synchros, which play a crucial role in the closed-loop control systems of permanent magnet synchronous machines (PMSMs). Compared to two-phase resolvers, three-phase synchros provide enhanced reliability by ensuring continued operation even in the event of an open-circuit fault. One of the key challenges in designing such sensors lies in selecting optimal windings and configurations while also developing efficient modeling techniques to minimize computational complexity. To address this issue, the study introduces a matrix-based method for designing wound rotor (WR) synchros. This approach allows for flexible configurations depending on the number of pole pairs and stator tooth counts. The proposed design methodology ensures adaptability and precision, making it a valuable tool for engineers working on electromagnetic sensor development. To validate the effectiveness of the proposed method, the Field Reconstruction Method (FRM) is employed, providing a fast and accurate modeling technique that can be implemented using MATLAB. Additionally, a comparative analysis is conducted with finite element analysis (FEA) to confirm the accuracy and reliability of the approach. Results demonstrate that the matrix-based method is an efficient and effective solution for optimizing WR synchro designs, significantly improving performance and computational efficiency.

Keywords: Analytical model, finite element method (FEM), synchro, wound rotor (WR).

1 Introduction

IN high-performance motion control systems for electrical machines, position sensors play a crucial role in ensuring precision and reliability. These sensors operate based on various technologies, including electromagnetic, optical, and resistive methods. Among them, optical and electromagnetic sensors are particularly favored due to their contactless operation and high accuracy [1]-[2]. Electromagnetic sensors, in particular, are highly suitable for demanding environments with significant temperature variations and strong vibrations [3]. These sensors are classified into two main categories: Hall-effect sensors and magnetic induction sensors. While Hall-effect sensors are less suitable for high-precision applications [4], magnetic induction sensors provide superior accuracy. Magnetic induction sensors are further divided into generator-type and transformer-type sensors. Transformer-type sensors excel in detecting small linear and rotary displacements, whereas linear and rotary selsyns are used for measuring larger motion ranges. Selsyns are categorized based on their core material and phase structure, with two primary types: air-core and ferromagnetic-core selsyns. Air-core selsyns, commonly referred to as "Inductosyns," and ferromagnetic-core selsyns, which include three-phase "Synchros" and two-phase "Resolvers," represent the most widely used variants. However, inductosyns are generally less preferred due to their lower induced voltage [5]. Functionally, selsyns operate on a principle similar to that of synchronous generators. Unlike generators, however, selsyn excitation windings are powered by high-frequency AC voltage. This results in Amplitude Modulation (AM) of the induced voltage in

Iranian Journal of Electrical & Electronic Engineering, 2025.
Paper first received 01 Mar. 2025 and accepted 11 Jun. 2025.
*Electrical Engineering Department, Sharif University of Technology, Tehran, Iran
E-mail: mohammadreza.eesazadeh@ee.sharif.edu.
E-mail: znasiri@sharif.edu
Corresponding Author: Zahra Nasiri-Gheidari.

the stator windings. The envelopes of these AM voltages are then processed by a synchro-to-digital converter (SDC) to determine the angular position [6].

To develop and manufacture these types of sensors, similar to electrical machines, a structured design process must be followed. Researchers utilize two primary approaches for predicting performance and optimizing electrical machines: numerical and analytical methods. Both are fundamentally derived from Maxwell's equations but differ in their advantages and limitations. Numerical methods, such as the finite element method (FEM) [8], offer high accuracy and can accommodate complex geometries and nonlinear material properties. However, they are often computationally intensive and less suitable for time-sensitive optimization tasks. In contrast, analytical methods, though generally less precise than numerical techniques, are computationally efficient and easier to implement, making them advantageous for rapid analysis. Given the focus on selsyns, it is important to explore analytical modeling techniques applied to their design and optimization. Various analytical methods have been proposed, each with distinct strengths and limitations in modeling. For instance, the magnetic equivalent circuit (MEC) model [9] has been successfully employed to predict the performance of different selsyn variants, including multi-turn resolvers [10]. Although the magnetic equivalent circuit (MEC) model offers a satisfactory simulation time, its accuracy is limited, particularly for variable reluctance (VR) resolvers. This limitation arises from the assumption that magnetic flux lines run parallel within the air gap, which does not hold for VR structures with significant variations in air-gap length or area. An alternative approach, the subdomain model [11], was applied in [12] to model a linear wound-field resolver. While this method provides highly accurate predictions of flux density in the air gap, accounting for longitudinal end effects and slotting, it is computationally demanding [12]. Moreover, the subdomain model is only effective for problems where boundary conditions align with one of the coordinate system axes [13], making it unsuitable for modeling VR selsyns with complex rotor geometries. Similarly, the winding function (WF) method [14] has been used for resolver modeling. However, like the MEC model, it assumes parallel flux paths in the air gap, limiting its accuracy in certain cases [15]. Additionally, several studies have investigated alternative approaches, such as the magneto-motive force-permeance (MMF-permeance) method [16] and the relative permeance method [17]. To overcome the challenges associated with analytical modeling of selsyns, this paper proposes the FRM for synchro analysis. Originally introduced in [18] and [19] for analyzing permanent magnet (PM) synchronous machines, FRM determines the air-gap magnetic flux density by summing the contributions of various sources, such as winding currents or permanent magnets, based on the principle of superposition. In this approach, fundamental functions derived from finite element method (FEM) simulations represent these flux contributions. Once obtained, these functions can be used to compute the magnetic field for any rotor position or winding current without requiring additional FEM simulations [20]-[21], significantly reducing computational effort. Moreover, FRM is simple to develop, quick to implement, and easily adaptable for various synchro configurations, making it a highly efficient modeling technique. Additionally, this paper presents a systematic approach for simplifying selection and configuring synchro windings, thereby optimizing both the design and manufacturing process. The proposed winding technique is adaptable to various pole-tooth configurations in WR-synchros. This method employs matrix calculus to transform the three-phase synchro signals into two components. If these components exhibit pure sinusoidal waveforms with minimal total harmonic distortion (THD), it ensures that the resulting three-phase system (synchro) performs optimally. This approach enables the precise design of winding arrangements to enhance overall performance.

2 Principle Operation of Synchro

Fig. 1 illustrates the fundamental operating principle of a synchro, a sensor commonly used for measuring angular positions. The device consists of four windings placed on ferromagnetic cores: one excitation winding and three output (signal) windings. The excitation winding plays a crucial role in generating the magnetic flux (φ_g) and is connected to an alternating current (AC) voltage source. The three signal windings are mechanically positioned at 120-degree intervals and interface with a synchro-to-digital converter (S2D). The S2D extracts position and speed data while exhibiting high input impedance, ensuring minimal current flow through the signal windings. As a result, the excitation current primarily determines the magnetic field within the synchro. When an AC voltage is applied to the excitation winding at a frequency significantly higher than the rotor speed ($2\pi f_s \gg \omega_r$), voltages are induced in the output windings. These induced voltages contain essential information for position estimation, making synchros reliable sensors in precision motion control applications. These induced voltages can be described using the following mathematical expressions [6]:

$$\zeta_{S1}(t,\theta) = \alpha U_m \sin\omega_r t \cos(\theta + 120^\circ) \quad (1)$$

$$\zeta_{S2}(t,\theta) = \alpha U_m \sin\omega_r t \cos(\theta) \quad (2)$$

$$\zeta_{S3}(t,\theta) = \alpha U_m \sin\omega_r t \cos(\theta - 120^\circ) \quad (3)$$

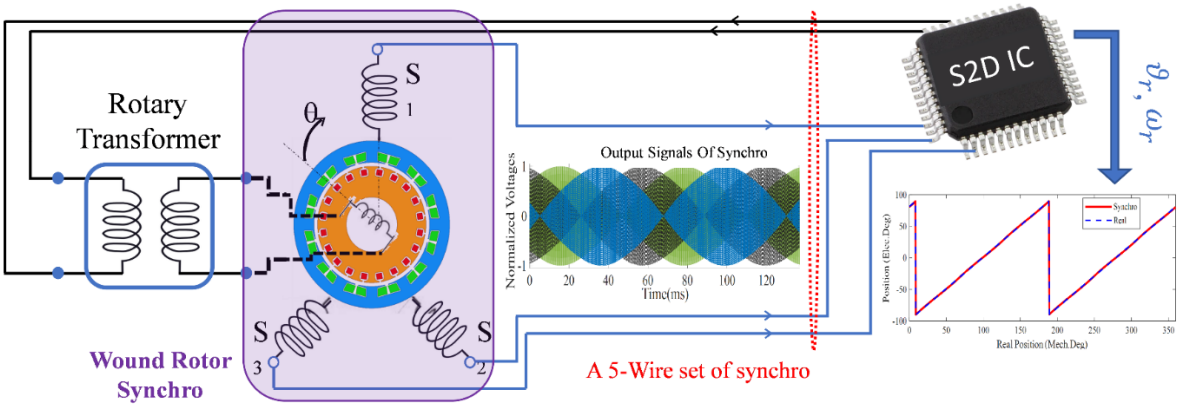

Fig 1. Principle operation of synchro.

Here, θ represents the position of rotor, α is the ratio of transformation of the synchro, $U_m$is amplitude of exciting voltage, and ζ_{S1}, ζ_{S2} and ζ_{S3} represent the induced voltages in the signal windings. The provided above equations describe the phase voltages of the synchro, which can be transformed into line voltages by computing the voltage differences between the terminals S3 and S1, S2 and S3, as well as S1 and S2. Further details on the simplification method can be found in [6]. The line voltage equations for the synchro are as follows, enabling the calculation of the rotor position.

$$\zeta_{S3-S1}(t,\vartheta) = U_m \sin\omega_r t \sin(\vartheta) \quad (1)$$

$$\zeta_{S2-S3}(t,\vartheta) = U_m \sin\omega_r t \sin(\vartheta + 120°) \quad (2)$$

$$\zeta_{S1-S2}(t,\vartheta) = U_m \sin\omega_r t \sin(\vartheta - 120°) \quad (3)$$

Generally, a synchro generates three sine waves, each separated by 120 degrees, all maintaining a uniform amplitude at the carrier frequency for any specified fixed spatial angle ϑ. By neglecting discrepancies, the following method can be used to determine the ratio of the amplitudes:

$$\frac{\zeta_{S3-S1}}{\zeta_{S2-S3}} = \frac{\sin(\vartheta)}{\sin(\vartheta + 120°)} \quad (4)$$

$$\frac{\zeta_{S2-S3}}{\zeta_{S1-S2}} = \frac{\sin(\vartheta + 120°)}{\sin(\vartheta - 120°)} \quad (5)$$

$$\frac{\zeta_{S1-S2}}{\zeta_{S3-S1}} = \frac{\sin(\vartheta - 120°)}{\sin(\vartheta)} \quad (6)$$

In conclusion, the placement of rotor (ϑ) can be determined using the following method:

$$\tan(\vartheta) = \frac{0.866}{\left(\frac{\zeta_{S3-S1}}{\zeta_{S2-S3}} + 0.5\right)} \quad (7)$$

Notably, if one of the synchro's phases is interrupted, the device's performance remains unaffected, and the shaft position can still be determined using the remaining two phases. This attribute significantly enhances the synchro's reliability.

3 Proposed Winding Technique

One of the most critical aspects of synchro design is selecting the winding type, configurations. The approach presented here is both comprehensive and efficient, eliminating the need for complex and time-consuming processes. To optimize the winding configuration of the WR synchro, that is assumed that the rotor winding follows the arrangement described in (11).

$$T_E(i) = T_{EM} \cos P\beta_i \quad (8)$$

where T_{EM} represents the maximum number of turns for excitation coil, and β_i the angular position of the rotor's i^{th} tooth:

$$\beta_i = \frac{2\pi}{z_r}(i-1) \quad (9)$$

This specific excitation coil generates a magnetic flux that interacts with the stator teeth, with its distribution varying based on the rotor position and the number of stator teeth, as in (13) [22]:

$$\varphi_s(k,\theta_r) = \varphi \cos P(\alpha_k - \vartheta) \quad (10)$$

In this scenario, φ represents an unchanging coefficient that correlates directly with the input current. It relies on the geometric parameters and remains unaffected by the position of rotor (ϑ). It is important to note that the input current in a synchro follows a sinusoidal waveform with a constant amplitude and a frequency significantly higher than the rotor's angular velocity $(d\vartheta/dt)$. Consequently, the induced voltage in a single turn of the k^{th} stator coil can be expressed as follows:

$$v_s(k,\vartheta) = \frac{d\varphi}{dt} \cos P(\alpha_k - \vartheta) \quad (11)$$

As a result, the voltage induced in the stator coils manifests as amplitude-modulated signals, where the carrier wave is given by $d\varphi/dt$. To extract the envelope of v_s, a demodulation block is integrated within Synchro-to-Digital Converters (SDCs), as follows:

$$\xi_s(k,\vartheta) = \xi\cos P_k(\alpha_k - \vartheta) \tag{12}$$

By utilizing trigonometric formulas:

$$\xi_s(k,\vartheta) = \xi_c(\vartheta)\cos P\alpha_k + \xi_s(\vartheta)\sin P\alpha_k \tag{13}$$

$$\xi_c(\vartheta) = \xi\cos P\vartheta \tag{14}$$

$$\xi_s(\vartheta) = \xi\sin P\vartheta \tag{15}$$

In this context, the $\xi_c$and ξ_s components are regarded as the target signals, representing the desired output for optimal winding configuration. The voltage induced in each stator coil, as formulated in (16), can be expressed in matrix form as follows:

$$\begin{bmatrix} \xi_s(1,\vartheta) \\ \vdots \\ \xi_s(k,\vartheta) \\ \vdots \\ \xi_s(z_s,\vartheta) \end{bmatrix} = \begin{bmatrix} 1 & 0 \\ \cos P\alpha_k & \sin P\alpha_k \\ \vdots & \vdots \\ \cos P\alpha_{z_s} & \sin P\alpha_{z_s} \end{bmatrix} \begin{bmatrix} \xi_c(\vartheta) \\ \xi_s(\vartheta) \end{bmatrix} \tag{16}$$

To maximize the utilization of all stator teeth in conventional wound rotor (WR) synchros, it is advisable to place a coil on each stator tooth. However, to form three windings, these coils must be interconnected in a manner similar to traditional WR synchros. This raises a key question: which coils should be interconnected, and how many turns should each coil have? By employing coils with an equal number of turns on each stator tooth, the left-hand side of (19) is obtained as a vector representation. The matrix on the right-hand side of (19) depends solely on the number of pole pairs in the synchro and the total number of stator teeth. Consequently, a system of z_s equations with two unknowns is established, allowing the desired results to be obtained by solving this system. To address the coil interconnection challenge, a mathematical approach is employed. By applying a constant multiplication to each row of (19) and summing the resulting equations, three new equations can be derived. For instance, in the case of a synchro with 12 stator slots, (19) can be rewritten as follows:

$$\begin{aligned} &\left[\xi_s(1,\theta_r)\cdots\xi_s(12,\theta_r)\right]^T = \frac{1}{2}\times \\ &\begin{bmatrix} 2 & \sqrt{3} & 1 & 0 & -1 & -\sqrt{3} & -2 & -\sqrt{3} & -1 & 0 & 1 & \sqrt{3} \\ 0 & 1 & \sqrt{3} & 2 & \sqrt{3} & 1 & 0 & -1 & -\sqrt{3} & -2 & -\sqrt{3} & -1 \end{bmatrix}^T \\ &\times \left[\xi_c(\vartheta) \quad \xi_s(\vartheta)\right]^T \end{aligned} \tag{17}$$

Various solutions can be derived to transform (20) into a new equation. One such solution is presented as follows:

$$\begin{bmatrix} Wind.\,1 \\ Wind.\,2 \\ Wind.\,3 \end{bmatrix} =$$

$$\begin{bmatrix} \xi_s(1,\vartheta) + \xi_s(2,\vartheta) + \xi_s(3,\vartheta) + \xi_s(4,\vartheta) \\ -\xi_s(5,\vartheta) - \xi_s(6,\vartheta) - \xi_s(7,\vartheta) - \xi_s(8,\vartheta) \\ \xi_s(9,\vartheta) + \xi_s(10,\vartheta) + \xi_s(11,\vartheta) + \xi_s(12,\vartheta) \end{bmatrix}$$

$$= \begin{bmatrix} 2.3660 & 2.3660 \\ 3.2321 & -0.8660 \\ 0.8660 & -3.2321 \end{bmatrix} \begin{bmatrix} \xi_c(\vartheta) \\ \xi_s(\vartheta) \end{bmatrix} \tag{18}$$

Above strategy is defined as Case 1 and Case 2 can be written as:

$$\begin{bmatrix} Wind.\,1 \\ Wind.\,2 \\ Wind.\,3 \end{bmatrix} =$$

$$\begin{bmatrix} \xi_s(1,\vartheta) + \xi_s(2,\vartheta) + \xi_s(7,\vartheta) - \xi_s(8,\vartheta) \\ +\xi_s(3,\vartheta) + \xi_s(4,\vartheta) + \xi_s(9,\vartheta) - \xi_s(10,\vartheta) \\ \xi_s(5,\vartheta) + \xi_s(6,\vartheta) + \xi_s(11,\vartheta) - \xi_s(12,\vartheta) \end{bmatrix}$$

$$= \begin{bmatrix} 1.7321 & 1 \\ 0 & 2 \\ -1.7321 & 1 \end{bmatrix} \begin{bmatrix} \xi_c(\vartheta) \\ \xi_s(\vartheta) \end{bmatrix} \tag{19}$$

Equations (21) and (22) demonstrate that the selected synchro winding configuration is optimized when the two components, $\xi_c$and ξ_s, exhibit the lowest THD. A closer examination of the given equation reveals a dimensional inconsistency in the matrices, preventing a direct solution. This issue arises because matrix inversion typically requires a square matrix. To overcome this limitation, an efficient method is proposed, as outlined in the following equation:

$$[W] = [S][E] \tag{20}$$

$$[S]^T[W] = [S]^T[S][E] \tag{21}$$

$$[G] = [S]^T[S] \tag{22}$$

$$[E] = [G]^{-1}[S]^T[W] \tag{23}$$

Where:

$$[W] = \begin{bmatrix} Wind.\,1 \\ Wind.\,2 \\ Wind.\,3 \end{bmatrix} \tag{24}$$

$$[S] = \begin{bmatrix} 1 & 0 \\ \cos P\alpha_k & \sin P\alpha_k \\ \vdots & \vdots \\ \cos P\alpha_{z_s} & \sin P\alpha_{z_s} \end{bmatrix} \tag{25}$$

$$[E] = \begin{bmatrix} \xi_c(\vartheta) \\ \xi_s(\vartheta) \end{bmatrix} \tag{26}$$

Under the assumption made in (21), it is recommended that each stator tooth is equipped with a single set of coils having an identical number of turns. Notably, the orientation of the coils on teeth #5 through #8 must be in

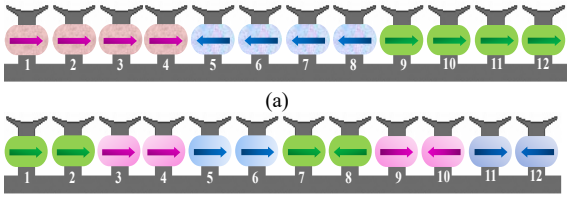

(a)

(b)

Fig. 2: Diagram illustrating the suggested winding technique: (a) Case 1 and (b) Case 2

contrast to the orientation of coils on the remaining teeth. Fig. 2 provides a visual representation of the stator of a WR synchro, showcasing the two different configurations of the proposed winding. The output signals ($\xi_c$and ξ_s) obtained from the converter for Case 1 are presented in Fig. 3(a). Likewise, the results for Case 2 have been extracted; however, as depicted in Fig. 3(b), the converter output in this case is suboptimal. These findings indicate that the winding configuration in Case 1 yields a more favorable synchro response.

4 Performance analysis of the WR-Synchro Based on proposed FRM

Synchros are engineered to operate with their ferromagnetic cores well below the saturation point on the B-H curve, typically around 10 mT [2]. This design strategy ensures that the cores retain linear magnetic characteristics, which justifies the employing the superposition principle in synchro modeling. As outlined in section II, the output windings connect to a synchro-to-digital converter (S2D) that possesses a high impedance in input, resulting in minimal current flow through these windings. Consequently, the magnetic field generated by the synchro is not influenced by the signal windings. Since the excitation coils primarily produce the magnetic field, the stator windings (signals) can be considered negligible during the calculation of the magnetic field. In other words, despite a 120-degree phase shift between the signal windings and the formation of mutual inductance between them, this mutual inductance does not significantly contribute to the creation of the magnetic field. To evaluate the flux linkage and the induced voltage within the output windings, post-processing techniques can be applied. Assuming linearity, the magnetic vector potential $\vec{\beta}$ can be represented as follows:

$$\vec{\beta}_2(r,\varphi,z) = \frac{i_{\text{exc2}}}{i_{\text{exc1}}}\vec{\beta}_1(r,\varphi,z) \tag{27}$$

In the cylindrical coordinate system, the coordinates (r,φ,z) denote the placement of τ at any chosen position. The magnetic vector potentials $\vec{\beta}_1$ and $\vec{\beta}_2$correspond to the excitation currents i_{excl} and i_{exc2} at a given position of rotor ϑ. Due to the symmetrical design of synchros, the magnetic vector potential exhibits periodic behavior concerning the rotor position for a specified excitation

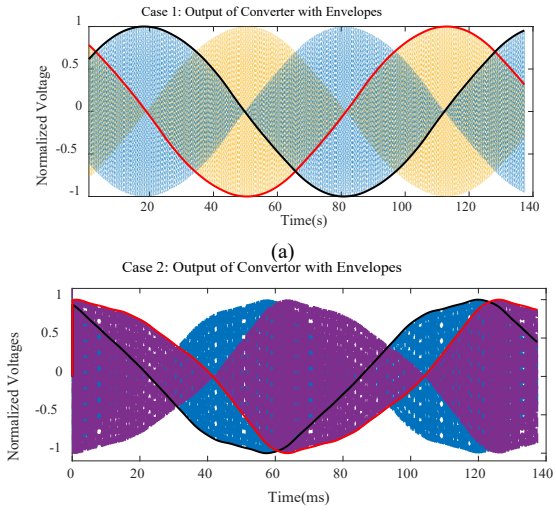

(a)

(b)

Fig. 3: Obtained from 2D FEA for the proposed winding of the studied WR-synchro, the output signals include: (a) Case 1- output of converter with envelopes and (b) Case 2- output of converter with envelopes

current. This means that if $\overrightarrow{\beta_1}$ and $\overrightarrow{\beta_{1,n}}$ represent the magnetic vector potentials for the i_{excl} at ϑ and $\vartheta + k\tau$, respectively, then:

$$\overrightarrow{\beta_{1,n}}(r,\varphi,z) = \beta_1(r,\varphi - k\tau,z) \tag{28}$$

here $k = 0,1,2,3,\dots,z_s - 1, \tau = (2\pi/z_s)$, $z_s$is the number of stator teeth, and τ represents the rotor's rotation for a WR synchros. Therefore, the vector potential of the magnetic field at any specified input current and rotor position can be derived by solving for the magnetic vector potential associated with a rotor

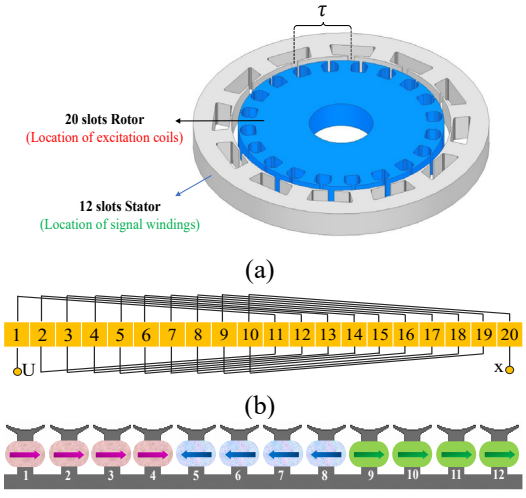

(a)

(b)

(c)

Fig. 4: (a) structure of studied WR synchro, excitation winding configuration, and (c) signals winding

rotation of τ using the specified excitation current, based on equations (11) and (12). These magnetic fields, referred to as basis functions, can be derived through either numerical or analytical methods. In this study, the basis functions are computed using FEM. Consequently, The FRM is called 2D-FRM when the fundamental functions are calculated using the 2D-FEM. This is further detailed in the subsequent sections.

In the WR synchro, as illustrated in Fig. 4(a), the magnetic field repeats after the rotor completes a rotation equivalent to the stator slot pitch, represented as $\tau = (2\pi/z_s)$. The excitation winding and signal windings, illustrated in Fig. 4(b) and (c). As a result, the fundamental functions can include both $L_{s,i}^{\text{basis}}$, and the L_r^{basis}. They play a key role in the modeling process. These basis functions are expressed as:

$$\begin{cases} L_r^{\text{basis}}(\vartheta); & 0 \le \vartheta \le \tau \\ L_{s,i}^{\text{basis}}(\vartheta); & 0 \le \vartheta < \tau \text{ and } i = 1,2,\dots,z_s \end{cases} \tag{29}$$

As described by equation (12), the L_r across all positions of rotor is expressed as:

$$L_r(\vartheta) = L_r^{\text{basis}}(\vartheta - \tau(i-1)); \tau(i-1) \le \vartheta < \tau i \tag{30}$$

For all rotor positions, the $L_{s,1}$ located on the first tooth of stator is expressed as follow:

$$L_{s,1}(\vartheta) = \begin{cases} L_{s,1}^{\text{basis}}(\vartheta); & 0 \le \vartheta < \tau \\ L_{s,z_s}^{\text{basis}}(\vartheta - \tau); & \tau \le \vartheta < 2\tau \\ L_{s,z_s-1}^{\text{basis}}(\vartheta - 2\tau); & 2\tau \le \vartheta < 3\tau \\ \vdots & \vdots \\ L_{s,2}^{\text{basis}}(\vartheta - (z_s-1)\tau); & (z_s-1)\tau \le \vartheta < 2\pi \end{cases} \tag{31}$$

Consequently, the mutual inductance relating to the input winding and any other stator tooth, $L_{s,i}(\vartheta)$, can be expressed as:

$$L_{s,j}(\vartheta) = L_{s,1}(\vartheta - \tau(j-1)); 0 \le \vartheta < 2\pi \tag{32}$$

Once the arrangement of the stator windings is identified, the mutual inductance, L_{signal}, which represents the interaction between the input winding and each respective output winding, can be calculated. This mutual inductance is defined by:

$$L_{\text{signal}}(\vartheta) = \sum_{i=1}^{z_s} T_{\text{signal}}(i) L_{s,i}(\vartheta) \tag{33}$$

Here, $T_{\text{signal}}(i)$ denotes the number of turns of the output coil located on the i^{th} tooth of stator. In this study, the number of turns in all coils across all the teeth is constant; however, their direction follows the pattern shown in Fig. 4(c) [6]. The calculation of the input current relies on the characteristics of the excitation winding, as shown in the follow:

$$v_{exc}(t) = R \times i_{exc}(t) + \frac{d}{dt}(L_r(\vartheta) \times i_{exc}(t)) \tag{35}$$

In this equation, v_{exc} and i_{exc} represent the terminal voltage and current, respectively, while the electrical resistance of the input winding denoted by R. As a result, the voltage induced in the output windings can be written as:

$$v_{signal}(t) = \frac{d}{dt}\left(L_{signal}(\vartheta) \times i_{exc}(t)\right) \tag{36}$$

It should be highlighted that the mutual inductance between each of the signal windings appears in the v_{signal} equation, due to the 120-degree phase shift between the windings. However, due to the negligible current in the signal windings, this mutual inductance has virtually no impact on the output voltage.

5 Model Verification

To assess the precision of the proposed method in forecasting the functionality of the synchro, we utilized 2D-FEM to derive the fundamental functions. We then compared the achieved results from the proposed 2D-FRM method with those of the 2D-FEM model. The FEM simulations was run using Ansys Electromagnetic Suite 21.2. The rotational speed of the synchro, ω_r, is typically significantly lower than its excitation frequency, f_s,. This allows for the assumption that the basis functions stay unchanged during each excitation period. Consequently, calculating the fundamental functions over a rotor rotation equivalent to one stator slot pitch, using a step size of (ω_r/f_s), is sufficient. In the case of the synchro studied here, the rotor speed is 480 r/min, and the excitation frequency is 5 kHz. Therefore, the period is 0.215 seconds. Since there are 12 slot pitches in one period, each slot pitch lasts for 10.4166 ms. In the simulations, the time step is set to 12.5 µs, meaning that approximately 834 static FEM simulations are needed for the full computation of fundamental functions. As previously stated, the basis for the fundamental functions is the L_r alongside the $L_{s,i}$. They are determined by injecting a steady current i_t into the input winding while the rotor is positioned at a specific angle (ϑ_0). The corresponding magnetic field is then determined by solving Maxwell's equations using the static FEM. From the resulting magnetic field, the λ_r and $\lambda_{s,i}$ are obtained. To find the L_r^{basis} and $L_{s,i}^{\text{basis}}$, the flux linkages are divided by the i_t, as described in the following equations:

$$\begin{aligned} L_r^{\text{basis}}(\vartheta_0) &= \frac{\lambda_r(\vartheta_0)}{i_t} \\ L_{s,i}^{\text{basis}}(\vartheta_0) &= \frac{\lambda_{s,i}(\vartheta_0)}{i_t}; i = 1,2,\dots,z_s \end{aligned} \tag{34}$$

This procedure is carried out for 834 different rotor positions, using a step size of approximately $^{30°}/_{834} \approx 0.036°$, ensuring coverage of the pitch of a single slot of stator. The fundamental functions derived from the 2D-FEM are employing to obtain the L_r and $L_{s,i}$ for the entire rotor rotation. Since the reconstructed inductances are discrete, Fourier series curve fitting is employed to interpolate the inductance values at other rotor positions. Following this, the induced voltage and input current in the output windings is computed using equations (18) and (19), which are solved using common numerical methods such as backward Euler as follow:

$$i_{\text{exc.}}^{k+1} = v_{\text{exc.}}^{k+1} \frac{\Delta t}{L_r^{k+1} + R\Delta t} + i_{\text{exc.}}^{k} \frac{L_r^{k}}{L_r^{k+1} + R\Delta t} \tag{37}$$

$$v_{\text{signal}}^{k+1} = \frac{L_{\text{signal}}^{k+1} \, l_{exc.}^{k+1} - L_{\text{signal}}^{k} \, l_{exc.}^{k}}{\Delta t} \tag{38}$$

Fig. 5(a) compares the input current obtained from the proposed FRM method with the results from the 2D-FEM. In addition, Fig. 5(b) shows the output voltages that is induced in the signal windings. The results indicate that the induced voltages from the FRM model closely match those from the 2D-FEM. Notably, the 2D-FEM simulation takes about 15 hours to complete, while the proposed FRM method only requires 59 minutes (plus 1 second for the reconstruction step), making it about 16 times faster. In 2D-FEM simulations, computational time is often extended due to factors such as high excitation frequency and a large number of meshes—in this particular case, the number of meshes is over 9600, and the excitation frequency is 5 kHz. An important point to consider is that the harmonics present within the range of the excitation frequency do not affect the performance of synchros. These harmonics are eliminated during the filtering process of the synchro's output signals when extracting the envelopes. Therefore, larger time steps can be used in calculating the inductances required for FRM simulations, which can significantly reduce the overall computational time. Also, in Maxwell Ansys, the calculation of inductances can be performed automatically through built-in software features. However, enabling these features often leads to longer simulation times because the automatic calculation involves the computation of mutual inductances between all coils. As an alternative method to reduce computational time, a fixed current I_{test} can be applied to the excitation coil, and the flux linkage with both the excitation coil and signal coils can be measured to compute the required inductances. In this method, dividing the flux linkage by the constant current yields the inductances., which directly eliminates the need to compute mutual inductances between the signal coils. As a result, the computational burden is reduced, and the simulation time for extracting the parameters in the FRM method is shortened. Furthermore, the position error comparison between the 2D-FEM and the FRM model, as presented in Table I, highlights the FRM's accuracy in predicting synchro performance. Additionally, the position error calculated from the 2D-FEM and 2D-FRM further demonstrates the effectiveness of the proposed model in predicting synchro performance, as illustrated in Fig. 5(c).

Table 1. Comparison results from 2D FEM and 2D FRM of WR Synchro Performance

	2D-FEM	2D-FRM	Deviation (%)
THD (%)	0.9594	0.9513	0.844
AAPE (Deg)	0.3980	0.3948	0.8
Simulation time	900 (min)	59 (min)	-

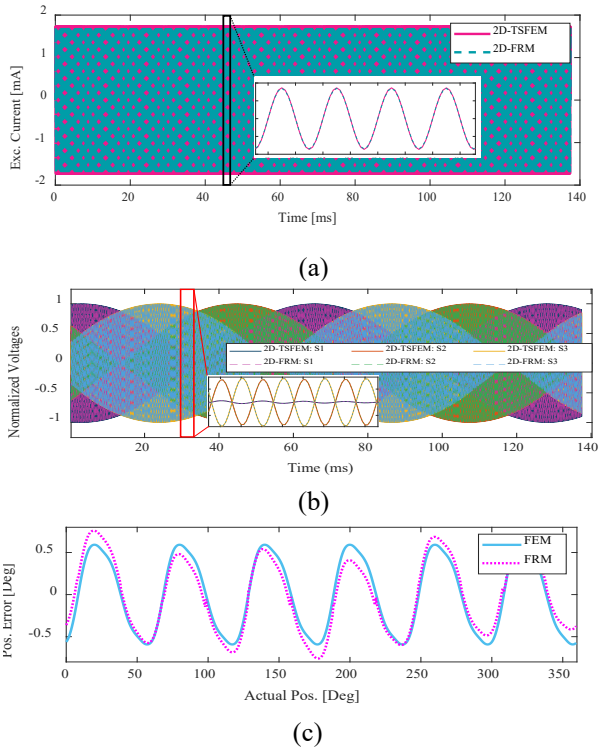

Fig. 5: Outcomes of the analyzed WR synchro derived from 2D-FEM and the proposed FRM.: (a) excitation current, (b) induced voltages, and (c) position error

6 Conclusion

This paper presents a structured approach to streamline the design and selection of synchro windings and functional modeling. The proposed method not only simplifies the process but also significantly reduces the time required for design and optimization. This method utilizes matrix calculations to map the selected synchro winding configuration into two fundamental components.

If these components exhibit minimal Total Harmonic Distortion (THD), it indicates that the optimal winding arrangement for the synchro has been achieved.
Additionally, this article presents the FRM as a method for modeling synchros. Initially, the principle behind the FRM method was explained, followed by its implementation for the WR synchro, particularly focusing on non-overlapping on-tooth windings. The fundamental functions of the FRM were calculated using the FEM, a well-established technique for analyzing electrical machines, including synchros. The outcomes of the proposed FRM model were subsequently compared to those derived from FEM simulations. For the WR synchro, the AAPE comparison revealed a deviation of less than 1%. Despite these small deviations, the FRM method significantly reduced simulation time, performing between 16 times faster than FEM. For instance, the simulation time for the WR synchro using FRM was 59 minutes. In conclusion, the FRM method serves as a powerful complementary tool to FEM for the analysis of synchros, particularly those with complex structures.

Conflict of Interest

The authors declare no conflict of interest.

Author Contributions

M. R. Eesazadeh:

1) *Idea & Conceptualization*
2) *Methodology and writing original draft*
3) *Software and Simulation*

Z. Nasiri-Gheidari:

1) *Idea & Conceptualization*
2) *Supervision*
3) *Review and editing*

References

[1] R. Tomassi. High-Reliability Position Control for Rugged Applications. Accessed: Nov. 22, 2021. [Online]. Available: https://www.ddc-web.com/resources/FileManager/syn_res/Synchro_Resolver_Technology_ WP.pdf

[2] Pancake Resolvers Handbook, Gen. Dyn. Mission Syst., Fairfax, VA, USA, Feb. 2020. [Online]. Available: https://www.gd-ots.com/wpcontent/uploads/2020/02/Pancake-Resolvers-Handbook_NAV_R.pdf .

[3] X. Ge, Z. Zhu, R. Ren, and J. Chen, "A novel variable reluctance resolver for HEV/EV applications," IEEE Trans. on Industry Applications, vol. 52, no. 4, pp. 2872-2880, 2016.

[4] X. Ge, Z. Q. Zhu, R. Ren, and J. T. Chen, "A Novel Variable Reluctance Resolver for HEV/EV Applications," IEEE Trans. on Industry Applications, vol. 52, no. 4, pp. 2872-2880, 2016, doi: 10.1109/TIA.2016.2533600.ees

[5] Saneie, Hamid, Zahra Nasiri-Gheidari, and Farid Tootoonchian. "Accuracy improvement in variable reluctance resolvers." IEEE Transactions on Energy Conversion 34, no. 3 (2019): 1563-1571.

[6] M. R. Eesazadeh and Z. Nasiri-Gheidari, "Winding Selection for Wound-Rotor Synchro," in *IEEE Sensors Journal*, vol. 24, no. 1, pp. 215-222, 1 Jan.1, 2024, doi: 10.1109/JSEN.2023.3332734.

[7] M.R. Eesazadeh, and Z. Nasiri Gheidari, “Proposal of Winding Arrangements for the WR Synchros to Facilitate the 3-phase to 2-phase Conversion without Scott-T Transformer,” presented at the POWER ELECTRONICS AND DRIVES: SYSTEMS AND TECHNOLOGIES CONFERENCE PEDSTC. 2024, Available: https://sid.ir/paper/1132492/en

[8] J. W. Jansen, J. P. C. Smeets, T. T. Overboom, J. M. M. Rovers, and E. A. Lomonova, “Overview of analytical models for the design of linear and planar motors,” IEEE Trans. Magn., vol. 50, no. 11, pp. 1–7, Nov. 2014, doi: 10.1109/TMAG.2014.2328556

[9] G. Forstner, A. Kugi, and W. Kemmetmuller, “A magnetic equivalent circuit based modeling framework for electric motors applied to a PMSM with winding short circuit,” IEEE Trans. Power Electron., vol. 35, no. 11, pp. 12285–12295, Nov. 2020.

[10] S. A. Seyed-Bouzari, M. R. Eesazadeh, F. Tootoonchian and Z. Nasiri-Gheidari, "Development of a Multiturn Linear Variable Reluctance Resolver With Integrated Ferromagnetic Core," in *IEEE Sensors Journal*, vol. 24, no. 19, pp. 29898-29905, 1 Oct.1, 2024, doi: 10.1109/JSEN.2024.3447232

[11] E. Roshandel, A. Mahmoudi, S. Kahourzade, and W. L. Soong, “Saturation consideration in modeling of the induction machine using subdomain technique to predict performance,” IEEE Trans. Ind. Appl., vol. 58, no. 1, pp. 261–272, Jan. 2022

[12] A. Paymozd, H. Saneie, Z. Nasiri-Gheidari and F. Tootoonchian, "Subdomain Model for Predicting the Performance of Linear Resolver Considering End Effect and Slotting Effect," in *IEEE Sensors Journal*, vol. 20, no. 24, pp. 14747-14755, 15 Dec.15, 2020, doi: 10.1109/JSEN.2020.3010785

[13] KhajueeZadeh, MohammadSadegh, Hamid Saneie, and Zahra Nasiri-Gheidari. "Development of a hybrid reference model for performance evaluation

of resolvers." *IEEE Transactions on Instrumentation and Measurement* 70 (2021): 1-8

[14] F. Zare and Z. Nasiri-Gheidari, "Winding Function Model for Predicting Performance of 2-DOF Wound Rotor Resolver," in *IEEE Transactions on Transportation Electrification*, vol. 8, no. 2, pp. 2062-2069, June 2022, doi: 10.1109/TTE.2021.3114210

[15] S. M. Raziee, O. Misir, and B. Ponick, "Winding function approach for winding analysis," IEEE Trans. Magn., vol. 53, no. 10, pp. 1–9, Oct. 2017.

[16] B. Gaussens et al., "Analytical armature reaction field prediction in field-excited flux-switching machines using an exact relative permeance function," IEEE Trans. Magn., vol. 49, no. 1, pp. 628–641, Jan. 2013.

[17] B. Gaussens, E. Hoang, O. de la Barriere, J. Saint-Michel, and M. Gabsi, "Analytical approach for air-gap modeling of field-excited flux-switching machine: No-load operation," IEEE Trans. Magn., vol. 48, no. 9, pp. 2505–2517, Sep. 2012

[18] W. Zhu, B. Fahimi, and S. Pekarek, "A field reconstruction method for optimal excitation of permanent magnet synchronous machines," IEEE Trans. Energy Convers., vol. 21, no. 2, pp. 305–313, Jun. 2006.

[19] A. Khoobroo, B. Fahimi, and S. D. Pekarek, "A new field reconstruction method for permanent magnet synchronous machines," in Proc. 34th Annu. Conf. IEEE Ind. Electron., Nov. 2008, pp. 2009–2013

[20] Saneie, Hamid, Zahra Nasiri-Gheidari, and Anouar Belahcen. "On the field-reconstruction method for electromagnetic modeling of resolvers." *IEEE Transactions on Instrumentation and Measurement* 72 (2022): 1-8.

[21] M.R. Eesazadeh, and Z. Nasiri Gheidari, "A Fast and Accurate Analytical Model for Performance Calculation of WR Synchros Based on Field Reconstruction Method," 2024 4th International Conference on Electrical Machines and Drives (ICEMD), Tehran, Iran, Islamic Republic of, 2024, pp. 1-6.

[22] K.-C. Kim, C. S. Jin, and J. Lee, "Magnetic shield design between interior permanent magnet synchronous motor and sensor for hybrid electric vehicle," IEEE Trans. Magn., vol. 45, no. 6, pp. 2835–2838, Jun. 2009

[23] H. Saneie, Z. Nasiri-Gheidari, and F. Tootoonchian, "Structural design and analysis of a high reliability multi-turn wound-rotor resolver for electric vehicle," *IEEE Transactions on Vehicular Technology,* vol. 69, no. 5, pp. 4992-4999, 2020.

Biography

Mohamad Reza Eesazadeh, was born in Ardabil, Iran, in 1994. He received the B.Sc. degree in electrical engineering from University of Mohaghegh Ardabili, Ardabil, Iran, in 2016, and M.Sc. degree in electrical engineering in 2020 from the Shahid Beheshti University, Tehran. He is currently working toward the Ph.D. degree in electrical engineering in Sharif University of Technology. His research focuses on modeling, design, and performance analysis of electrical machines and electromagnetic sensors.

Zahra Nasiri-Gheidari received the B.Sc. degree from the Iran University of Science and Technology, Tehran, Iran, in 2004, and the M.Sc. and Ph.D. degrees from University of Tehran, Tehran, in 2006 and 2012, respectively, all in electrical engineering. She is currently a Professor in the Department of Electrical Engineering at Sharif University of Technology. Her research focuses on the design, optimization, and performance analysis of electrical machines and electromagnetic sensors.